Оптический журнал

Оптическое приборостроение

Лавинные фотодетекторы на основе InGaAs/InAlAs, интегрированные с волноводными структурами «кремний на изоляторе»

© 2017 г. Dongdong Yin*, **; Xiaohong Yang*, **; Tingting He*, **; Qianqian Lv*, **; Han Ye*, **, Qin Han*,**

*State Key Laboratory on Integrated Optoelectronics, Institute of Semiconductors, Chinese Academy of Sciences, Beijing, People's Republic of China
**College of Materials Science and Opto-Electronic Technology, University of Chinese Academy of Sciences, Beijing, People's Republic of China

E-mail: xhyang@semi.ac.cn

Выполнено моделирование лавинных фотодиодов на основе InGaAs/InAlAs, оптическая связь которых с волноводными структурами «кремний на изоляторе» осуществлялась посредством убегающих волн, проходящих через связующий слой бензоциклобутена. Для передачи света из волокна к кремниевому волноводу использован кремниевый соединитель на основе дифракционной решетки на волокне. При моделировании проводилась оптимизация эффективности оптической связи для различных толщин слоя бензоциклобутена, параметров слоя InP и ширины кремниевого волновода. Результаты моделирования показали достижимость эффективности детектирования 96,7% в условиях толщины кремниевого волновода 2 мкм и размера фотодетектора 40 мкм при значении произведения усиления на полосу пропускания 135 ГГц на длине волны 1550 нм.

Ключевые слова: *кремний на изоляторе, лавинный фотодетектор, убегающие волны, бензоциклобутеновое связующее.*

InGaAs/InAlAs avalanche photodetectors integrated on silicon-on-insulator waveguide circuits

© 2017 Dongdong Yin*, **; Xiaohong Yang*, **; Tingting He*, **; Qianqian Lv*, **; Han Ye*, **, Qin Han*,**

*State Key Laboratory on Integrated Optoelectronics, Institute of Semiconductors, Chinese Academy of Sciences, Beijing, People's Republic of China
**College of Materials Science and Opto-Electronic Technology, University of Chinese Academy of Sciences, Beijing, People's Republic of China

E-mail: xhyang@semi.ac.cn

Submitted 01.02.2016

We simulated an evanescently coupled InGaAs/InAlAs avalanche photodetector integrated on silicon-on-insulator waveguide circuits using benzocyclobutene as the bonding layer. A silicon fiber-grating coupler is adopted to couple light from the fiber to the Si waveguide and light can finally be absorbed in the absorption region. Simulations around improving the optical coupling efficiency with different device dimensions such as different benzocyclobutene bonding thicknesses, different InP layer parameters and different silicon waveguide widths were carried out. The simulation result shows a detection efficiency of 96.7% for 2 μm silicon waveguide device with a photodetector length of 40 μm which can get a gain-bandwidth product of 135 GHz at 1550 nm.

Keywords: *silicon-on-insulator, avalanche photodetector, evanescent wave, benzocyclobutene bonding.*

OCIS codes: *040.1345, 040.5160, 130.5990, 200.4650*

1. INTRODUCTION

Over the past fifty years, avalanche photodetector (APD) that converts optical signals into the electrical domains for further signal processing and data manipulation has been widely used in business, military and scientific research. In recent years, the motivation to research APD comes from the optical communication. Because of the internal gain, APD can achieve higher sensitivity than PIN photodetector [1–3] and is mainly used for the detection of weak signal in long distance optical fiber communication. The InAlAs material is lattice matched with InP and has a low ionization coefficient ratio α_p/α_n of 0.3–0.4 under the electric field of 400–650 KV/cm [4]. Nowadays, almost all the high speed APD uses InAlAs material as the multiplication layer.

Silicon is transparent at the optical communication wavelength and can be used as an excellent wave guiding material due to its low loss. Besides, the large index contrast of silicon with silicon dioxide cladding layer of the silicon-on-insulator (SOI) circuits results in highly confined optical modes. At present, researches on silicon photonics [5–10] have been focused on realizing various components of photonic integrated circuits, including active photonic devices such as lasers [11], modulators [12], and photodetectors (PDs) [13] as well as passive waveguide devices based on the processed SOI platform. However, the huge optical loss is the main restriction of the overall performance of the photonic chip. Integrating an APD instead of a PIN PD onto the SOI circuits is one way to solve the problem. Moreover, the research on integrated APDs can be of great significance in the quantum communication [14, 15].

The InGaAs/InAlAs APDs integrated on the SOI circuits haven't been reported to the best of our knowledge. High gain-bandwidth (GB) product of 320 GHz of the III–V waveguide APD was achieved, however the efficiency was only 16% [16]. A higher efficiency of 94% using the antireflex coating was obtained with a GB product of 110 GHz [17]. The Ge/Si waveguide APD with a GB product of 105 GHz and a primary responsivity of 0.8 A/W equivalent to an efficiency of 64% was also demonstrated for the advantage of complete compatibility with CMOS processes [18]. All of the results above were obtained at the wavelength of 1550 nm. The dark current of the Ge/Si APD was higher compared with InGaAs/InAlAs APD and the absorption coefficient of germanium drops rapidly beyond 1550 nm inhibiting its application for *L* band. Growing high-quality pure Ge film on Si was also a key challenge because of the lattice mismatch. In this paper, we present the simulated optimizations of an evanescently coupled APD integrated on SOI with the benzocyclobutene (BCB) bonding method [19–22]. The strong optical modes confinement of the silicon waveguide on the SOI and the large coupling efficiency between the APD absorption layer and the silicon waveguide result in a high efficiency of the integrated APD. The simulation result shows an efficiency of 96.7% and a GB product of 135 GHz for the 2 μm silicon waveguide device with a PD length of 40 μm at 1550 nm. The factors that affect the light coupling efficiency such as silicon waveguide width, BCB bonding thicknesses and InP layer parameters are optimized.

2. DEVICE STRUCTURE DESIGN

Figures 1a, b show the schematic of the cross section view and side view of the integrated APD. A silicon fiber-grating coupler with a ridge silicon waveguide is used to realize the light coupling from fiber to the silicon ridge waveguide. The silicon grating layer is designed with a top silicon layer thickness of 340 nm and an etching depth of 200 nm. For 340 nm top silicon layer of the SOI waveguide, the grating can be etched deeper, which will not bring great reflection. Then, more light can be diffracted out from the waveguide. A BCB bonding method is adopted to accomplish the integration of the unprocessed III–V epitaxial film and the SOI.

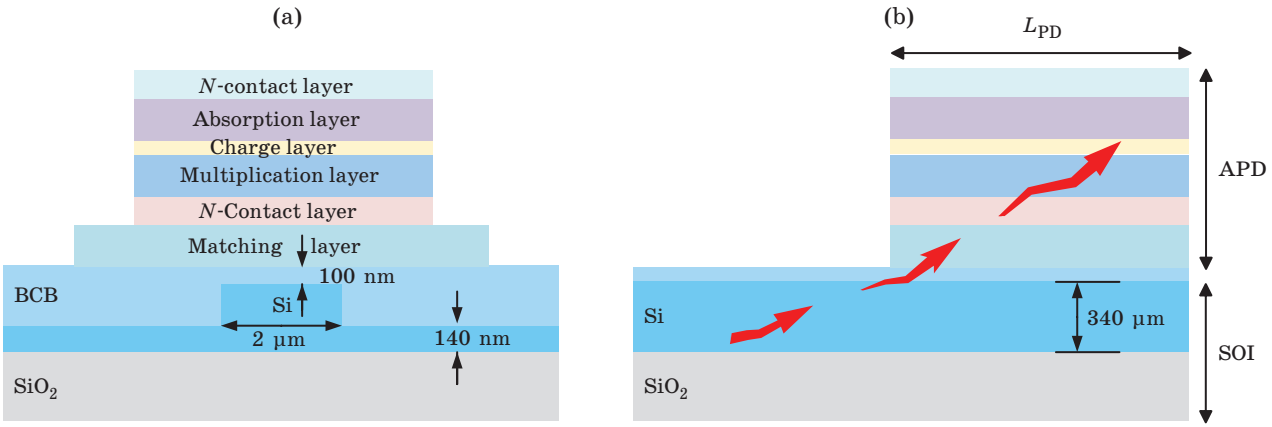

Fig. 1. The cross section view (a) and side view (b) of the integrated APD. The APD is stacked on top of the BCB bonding layer, which is used to accomplish the integration of the Si waveguide and the APD.

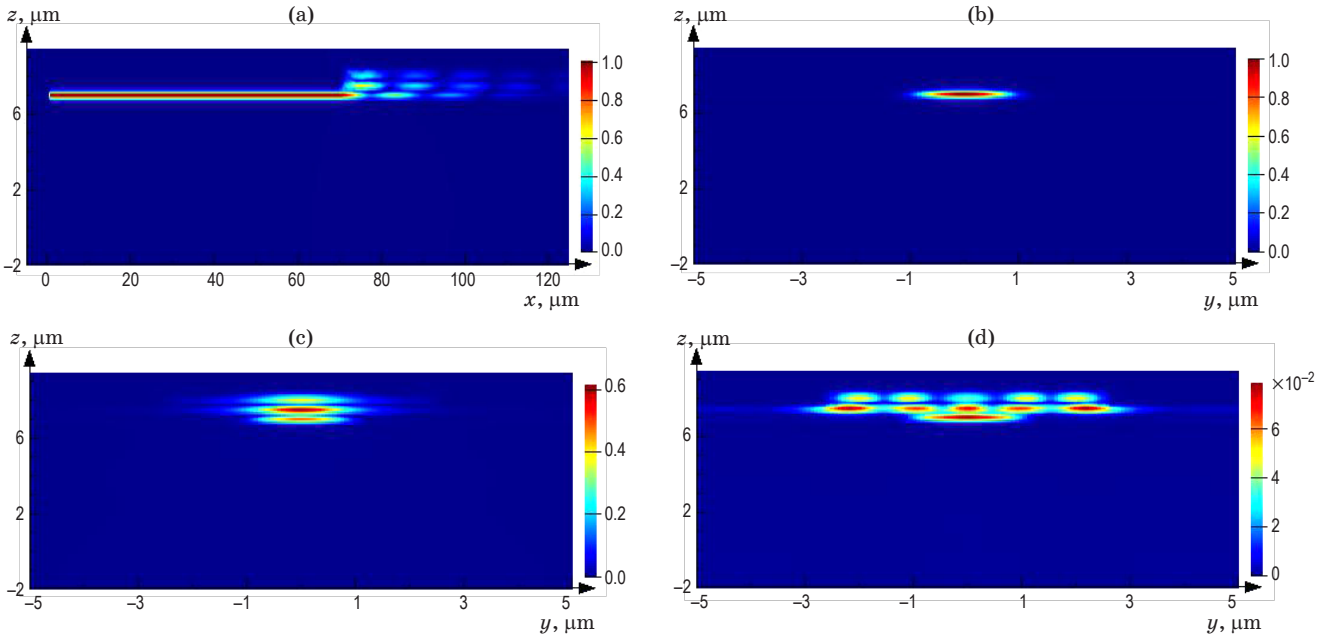

Fig. 2. (a) The lateral optical field distribution of the simulation result of the device, (b) the cross section of the optical field distribution in the Si waveguide, (c) the cross section of the optical field distribution at the detection region of 5 μm, (d) the cross section of the optical field distribution at the detection region of 40 μm.

The epitaxial layer structure of the avalanche photodetector

Function	Compound	n	d, μm
substract	i-InP	3.146	500
Buffer layer	i-InP	3.146	0.1
p-contact	p^+-$InGa_{0.53}As_{0.47}$	3.56	0.08
	p^+-InP	3.146	0.2
Grading	i-$InGa_{0.11}As_{0.25}P$	3.26	0.02
Cladding	i-$InGa_{0.34}As_{0.73}P$	3.44	0.02
Absorption	i-$InGa_{0.53}As_{0.47}$	3.56–i0.086	0.2
Graded layer	i-InGaAlAs	3.3	0.03
Charge	p-$In_{0.52}Al_{0.48}As$	3.23	0.06
Multiplication	i-$In_{0.52}Al_{0.48}As$	3.23	0.15
n-contact	n^+-$In_{0.52}Al_{0.48}As$	3.23	0.01
Etch-stop	n^+-InP	3.146	0.01
Matching layer	n^+-InGaAsP	3.41	0.32

The III–V epitaxial structure is grown on an InP substrate. The APD structure utilizes a separate absorption, grading and multiplication structure and the epitaxial layer structure parameter is shown in Table. A thin InGaAs absorption layer and InAlAs multiplication layer can reduce the carrier transit time and multiplicative noise of the device, which can get a high speed and high response of APD. In the simulation, a 320 nm n^+-$InGa_{0.3}As_{0.64}P$ layer is used as the light matching layer. A non-intentionally doped $In_{0.53}Ga_{0.47}As$ is designed to be the absorption layer. The low ionization coefficient ratio of InAlAs can effectively reduce the excess noise and improve the response speed of the device. Besides, its wide bandgap can restrain the tunneling current. Therefore, a 150 nm non-intentionally doped $In_{0.52}Al_{0.48}As$ layer is used as the multiplication layer. The grading layer is used to improve the bandwidth performance caused by the big bandgap difference as well as reducing the reflection caused by the large refractive index difference of the absorption layer and the multiplication layer. And a charge layer is taken to control the electric field distribution of the multiplication layer and absorption layer.

Light in fiber is first coupled into the silicon waveguide, then is coupled gradually upwards and is finally absorbed by the absorption layer. The optical field distribution of the simulation result of the device with a final BCB thickness of 100 nm and a silicon waveguide width of 2000 nm is shown in Fig. 2.

3. SIMULATIONS AND DISSCUSIONS

The simulations were conducted at 1550 nm. The simulated device structure began with an InP layer thickness of 250 nm. On this layer an InP waveguide was used to couple light in the silicon waveguide into the photodetection region as shown in Fig. 3. The InP waveguide had an initial width (W_{InP}) and length (L_w) of 2 and 14 μm. At the end of the InP waveguide followed an InP trapezoidal taper to help light in the InP waveguide dispersed uniformly among the whole detection width range. The InP taper had a length (L_t) of 6 μm with width from 2 to 5 μm. Light out from the fiber was first diffracted into the silicon grating

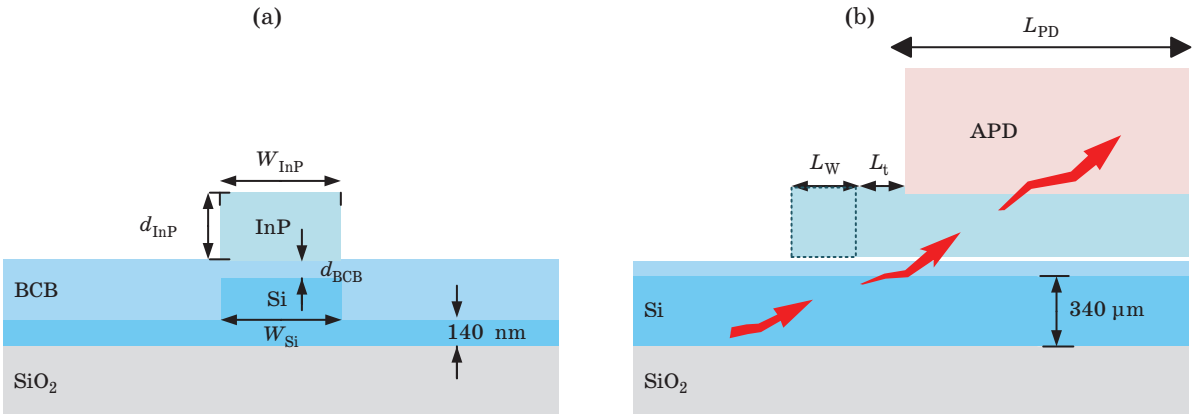

Fig. 3. The cross section view (a) and side view (b) of the starting integrated APD structure with an InP waveguide layer.

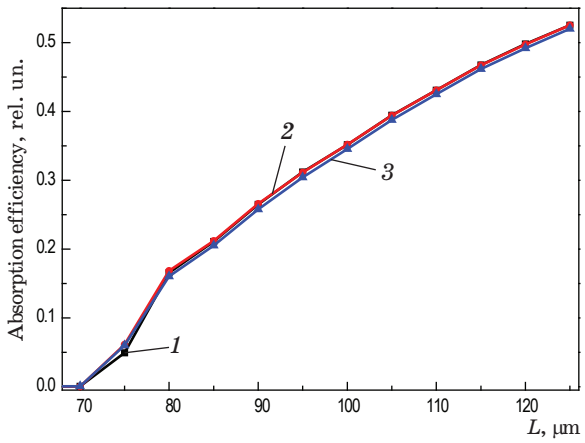

Fig. 4. The absorption efficiency curves of the device with different InP stripe waveguide widths W_{InP} (*1* – 1.5, *2* – 2, *3* – 2.5 μm). The absorption region starts at the location of 70 μm.

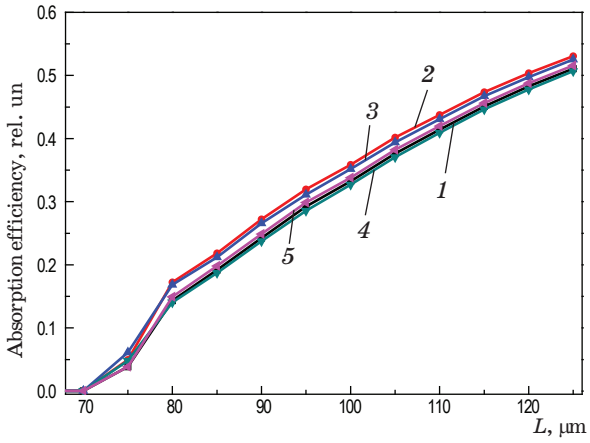

Fig. 5. The absorption efficiency curves of the device with different InP stripe waveguide lengths L_t (*1* – 10, *2* – 12, *3* – 14, *4* – 16, *5* – 18 μm).

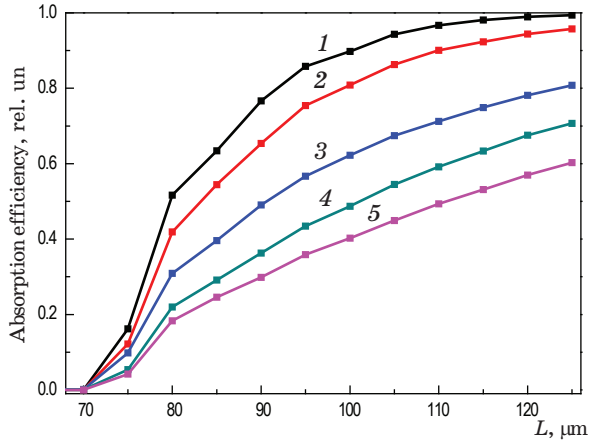

Fig. 6. The absorption efficiency curves of the device with InP layer thickness d_{InP} of 0 (*1*), 50 (*2*), 100 (*3*), 150 (*4*), 200 nm (*5*).

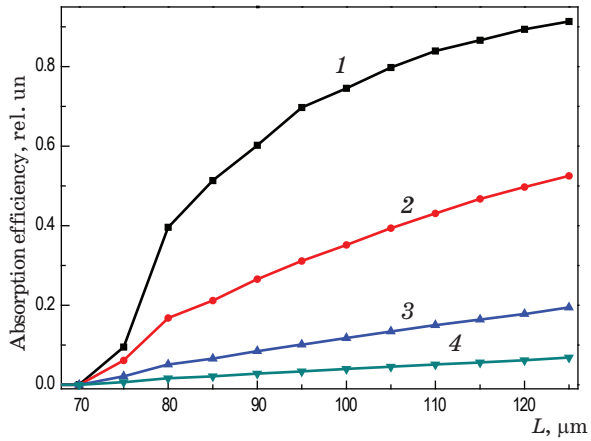

Fig. 7. The absorption efficiency curves of the device with BCB thicknesses d_{BCB} of 50 (*1*), 100 (*2*), 150 (*3*), and 200 nm (*4*).

coupler and could finally spread steadily in the Si waveguide after propagating a distance. The light in the silicon bus waveguide was evanescently coupled into the active region like a direction coupler. The light was absorbed evenly along the absorption region which could improve the response of the device and the power characteristics of the device. Simulations of the coupling efficiency of the integrated APD with different InP guiding layer structures, different BCB thicknesses and different silicon waveguide widths were conducted. The simulated device length of the absorption region (L_{PD}) was 55 μm.

Figures 4 and 5 showed the absorption efficiency of the device with different InP waveguide widths W_{InP} and lengths L_t. Figure 4 indicated that the InP waveguide widths had very small effect on absorption efficiency of the device with an InP waveguide layer thickness d_{InP} of 250 nm. Light oscillated between the InP waveguide and the silicon waveguide. Figure 5 showed that the InP waveguide with a 12 μm length got the highest efficiency of 53% with a device length L_{PD} of 55 μm which was 51, 50.7, 52.5, 50.7, and 51.6% for 10, 13, 14, 16, and 18 μm length device respectively. On this basis, simulations with different InP layer thicknesses were conducted.

Figure 6 showed the absorption efficiency curve of the device with different InP thicknesses. The absorption efficiency of the device increased with d_{InP} getting smaller. The device achieved an efficiency of 96.7% without InP layer which was 95.7, 80.8, 70.7, 60.2, and 52.5% for 50, 100, 150, 200, and 250 nm d_{InP} device. The simulation result showed that the InP guiding layer could be removed.

Then, different BCB thicknesses (d_{BCB}) of 50, 100, 150, and 200 nm were simulated. The simulation results presented that the thinner the BCB thickness was, the faster the light was absorbed when the BCB thickness was more than 100 nm. Light in the silicon waveguide could be absorbed faster for 50 nm BCB thickness device at the starting of the absorption region than the 100 nm BCB thickness device. The 100 nm BCB thickness device could absorb light fast after a detection length of 20 μm. The detailed absorption efficiency of the device with different d_{BCB} was shown in Fig. 7. Device with the d_{BCB} of 50, 100, 150, and 200 nm could get an efficiency of 96.7, 99.4, 93.0, and 62.1% at the detection location of 55 μm respectively. Considering the coupling efficiency and the difficulty of the bonding process, the d_{BCB} of 100 nm was used.

Finally, the simulation of the integrated PD getting rid of the InP layer with different silicon waveguide widths was conducted. The absorption efficiency curve of the device with different silicon waveguide widths of 450 nm, 1 and 2 μm was shown in Fig. 8. The coupling between the silicon waveguide and the detection region almost made no difference for devices with different silicon waveguide widths. It indicated that the coupling was no longer limited

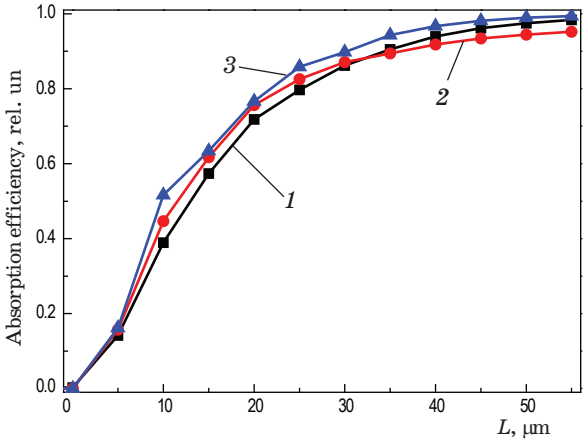

Fig. 8. The absorption efficiency curves of the device with different silicon waveguide widths (*1* – 450 nm, *2* – 1 μm, *3* – 2 μm) after the InP layer had been removed.

by the light mode in the silicon waveguide which should match the light mode of the InP waveguide. Considering the low loss property of the wide silicon waveguide, the silicon waveguide width we used was 2 μm. The final coupling efficiency of the device was 96.7 and 99.4% with a detection length of 40 and 55 μm respectively. To achieve a tradeoff between efficiency and bandwidth, we chose a final PD length of 40 μm. The GBP of the device is given as the form

$$M \bullet B = \frac{1}{2\pi N(\alpha_p/\alpha_n)\tau_{av}},$$

where N is the function of α_p/α_n and τ_{av} is the average transit time of electron and hole [23]. The calculated GBP of the device was 135 GHz. The calculated GBP of the device was 135 GHz.

To obtain a high performance APD, the InP layer thickness d_{InP} and the BCB bonding thickness d_{BCB} were the main factors that affected the efficiency of the device. The InP waveguide width W_{InP} and length L_t had small influence on the coupling efficiency. The detection efficiency of the 40 μm long device with a BCB thickness of 100 nm and a silicon waveguide width of 2 μm was 96.7% when the InP layer was removed. The theoretical GBP of the integrated PD was 135 GHz.

4. CONCLUSION

We present an evanescently coupled waveguide APD integrated on the 2 μm silicon waveguide. A final device structure is designed with a BCB bonding thickness of 100 nm. The InP guiding layer is removed. The final high detection efficiency and GB product are 96.7% and 135 GHz for device with the length of 40 μm at the wavelength of 1550 nm. The integrated avalanche photodetector is promising to be used in the silicon photonic chip and the quantum communication.

Please replace the last paragraph as the corrected one.

REFERENCES

1. *Personick S.D.* Receiver design for digital fiber optic communication systems, I // Bell Syst. Tech. J. 1973. V. 52. P. 843.
2. *Forrest S.R.* Sensitivity of avalanche photodetector receivers for high-bit-rate long-wavelength optical communication systems // Semiconduct. Semimet. 1985. V. 22. P. 329.
3. *Kasper B.L., Campbell J.C.* Multigigabit per-second avalanche photodiode lightwave receivers // J. Light Technol. 1987. V. 5. P. 1351.
4. *Watanabe I., Torikai T., Makita K., Fukushima K., Uji T.* Impact ionization rates in (100) $Al_{(0.48)}In_{(0.52)}As$ // IEEE Electr. Device L. 1990. V. 11. P. 437.
5. *Absil P.P., Verheyen P., Heyn P.D., Pantouvaki M., Lepage G., Coster J.D., Campenhout J.V.* Silicon photonics integrated circuits: A manufacturing platform for high density, low power optical I/O's // Opt. Exp. 2015. V. 23. P. 9369.
6. *Sui S., Tang M., Yang Y., Xiao J., Du Y., Huang Y.* Mode investigation for hybrid microring lasers with sloped sidewalls coupled to a silicon waveguide // IEEE Photon. J. 2015. V. 7. P. 1.
7. *Streshinsky M., Ding R., Liu Y., Novack A., Galland C., Lim A.E.J., Guo-Qiang Lo P., Baehr-Jones T., Hochberg M.* The road to affordable, large-scale silicon photonics // Opt. Photon. News. 2013. V. 24. P. 32.
8. *Baehr-Jones T., Pinguet T., Lo P.G.Q., Danziger S., Prather D., Hochberg M.* Myths and rumours of silicon photonics // Nat. Photon. 2012. V. 6. P. 206.
9. *Heck M.J.R., Chen H.W., Fang A.W., Koch B.R., Liang D., Park H., Sysak M.N., Bowers J.E.* Hybrid silicon photonics for optical interconnects // IEEE J. Sel. Topics Quantum Electron. 2011. V. 17. P. 333.
10. *Ohira K., Kobayashi K., Iizuka N., Yoshida H., Ezaki M., Uemura H., Kojima A., Nakamura K., Furuyama H., Shibata H.* On-chip optical interconnection by using integrated III–V laser diode and photodetector with silicon waveguide // Opt. Exp. 2010. V. 18. P. 15440.
11. *Boyraz O., Jalali B.* Demonstration of a silicon Raman laser // Opt. Exp. 2004. V. 12. P. 5269.
12. *Liu A., Liao L., Rubin D., Nguyen H., Ciftcioglu B., Chetrit Y., Izhaky N., Paniccia M.* High-speed optical modulation based on carrier depletion in a silicon waveguide // Opt. Exp. 2007. V. 15. P. 660.
13. *Campenhout J.V., Binetti P.R.A., Romeo P.R., Regreny P., Seassal C., Leijtens X.J.M., Vries T.D.* Low-footprint optical interconnect on an SOI chip through heterogeneous integration of InP-based microdisk lasers and microdetectors // IEEE Photonics Technol. Lett. 2009. V. 21. P. 522.
14. *Chunnilall C.J., Lepert G., Allerton J.J., Hart C.J., Sinclair A.G.* Traceable metrology for characterizing quantum optical communication devices // Metrologia. 2014. V. 51. P. S258.
15. *Gisin N., Thew R.* Quantum communication // Nature Photon. 2007. V. 1. P. 165.
16. *Kinsey G.S., Campbell J.C., Dentai A.G.* Waveguide avalanche photodiode operating at 1.55 μm with a gain-bandwidth product of 320 GHz // IEEE Photonic. Tech. L. 2001. V. 13. P. 842.
17. *Shiba K., Nakata T., Takeuchi T., Sasaki T., Makita K.* 10 Gbit/s asymmetric waveguide APD with high sensitivity of 30 dBm // Electron. Lett. 2006. V. 42. P. 1177.
18. *Ang K.W., Lo P.G.Q.* Avalanche photodetectors: Si charge avalanche enhances APD sensitivity beyond 100 GHz // Laser Focus World. 2010. V. 46.
19. *Keyvaninia S., Muneeb M., Stankovi S., Van Veldhoven P.J., Van Thourhout D., Roelkens G.* Ultra-thin DVS-BCB adhesive bonding of III–V wafers, dies and multiple dies to a patterned silicon-on-insulator substrate // Opt. Mat. Exp. 2013. V. 3. P. 35.
20. *Roelkens G., Liu L., Liang D., Jones R., Fang A., Koch B., Bowers J.* III–V/silicon photonics for on-chip and intra-chip optical interconnects // Laser & Photon. Rev. 2010. V. 4. P. 751.
21. *Sheng Z., Liu L., Brouckaert J., He S.L., Thourhout D.V.* InGaAs PIN photodetectors integrated on silicon-on-insulator waveguides // Opt. Exp. 2010. V. 18. P. 1757.
22. *Liang D., Roelkens G., Baets R., Bowers J.E.* Hybrid integrated platforms for silicon photonics // Mat. 2010. V. 3. P. 1782.
23. *Emmons R.B.* Avalanche-photodiode frequency response // J. Appl. Phys. 1967. V. 38. P. 3705.